ADVANCED BIOSYSTEMS
www.adv-biosys.com

Targeting and Modulation of Liver Myeloid Immune Cells by Hard-Shell Microbubbles

*Klaudia T. Warzecha, Matthias Bartneck, Diana Möckel, Lia Appold, Can Ergen, Wa'el Al Rawashdeh, Felix Gremse, Patricia M. Niemietz, Willi Jahnen-Dechent, Christian Trautwein, Fabian Kiessling, Twan Lammers, and Frank Tacke**

Poly *n*-butylcyanoacrylate (PBCA)-based hard-shell microbubbles (MB) have manifold biomedical applications, including targeted drug delivery or contrast agents for ultrasound (US)-based liver imaging. MB and their fragments accumulate in phagocytes, especially in the liver, but it is unclear if MB affect the function of these immune cells. Herein, it is shown that human primary monocytes internalize different PBCA-MB by phagocytosis, which transiently inhibits monocyte migration in vertical chemotaxis assays and renders monocytes susceptible to cytotoxic effects of MB during US-guided destruction. Conversely, human macrophage viability and function, including cytokine release and polarization, remain unaffected after MB uptake. After intravenous injection in mice, MB predominantly accumulate in liver, especially in hepatic phagocytes (monocytes and Kupffer cells). Despite efficiently targeting myeloid immune cells in liver, MB or MB after US-elicited burst do not cause overt hepatotoxicity or inflammation. Furthermore, MB application with or without US-guided burst does not aggravate the course of experimental liver injury in mice or the inflammatory response to liver injury in vivo. In conclusion, PBCA-MB have immunomodulatory effects on primary human myeloid cells in vitro, but do not provoke hepatotoxicity, inflammation or altered response to liver injury in vivo, suggesting the safety of these MB for diagnostic and therapeutic purposes.

1. Introduction

Microbubbles (MB) are gas-filled vesicles sizing from 1–5 µm with a shell composed of proteins, lipids (soft-shell MB) or polymers (hard-shell MB). They are routinely used as contrast agents in ultrasound (US) imaging, especially in liver imaging for diagnosing benign or malignant hepatic tumors.[1,2] The shell composition plays a pivotal role for circulation time, stability (physical and chemical), as well as for oscillation during US treatment. Imaging of flexible soft-shell MB is mostly done using nondestructive US, which is based on nonlinear oscillation upon exposition to low- and medium intensity US pulses. Hard-shell MB such as those based on poly *n*-butylcyanoacrylate (PBCA) show less nonlinear responses but higher backscattering properties, which can be of advantage for imaging at higher frequencies where the nonlinear contrast modes are less effective.[3]

Although at present soft-shell MB are primarily used in clinical evaluation,[4] hard-shell MB might provide more diverse options for drug loading and multifunctionality because of their much thicker shell and the option of US-directed MB destruction allowing image-guided local drug release.[3,5] Additionally, hard-shell MB only exhibit a marginal complement activation (lower than soft-shell MB) underlining their biocompatibility.[6] Nevertheless, limited knowledge exists on the immunomodulatory effects of hard-shell MB on

K. T. Warzecha, Dr. M. Bartneck, C. Ergen, P. M. Niemietz, Prof. C. Trautwein, Prof. F. Tacke
Department of Medicine III
Medical Faculty
University Hospital Aachen
Pauwelsstraße 30, 52074 Aachen, Germany
E-mail: frank.tacke@gmx.net

D. Möckel, L. Appold, Dr. W. Al Rawashdeh, Dr. F. Gremse, Prof. F. Kiessling, Prof. T. Lammers
Department of Experimental Molecular Imaging
University Hospital and Helmholtz Institute for Biomedical Engineering
RWTH Aachen University
52074 Aachen, Germany

The ORCID identification number(s) for the author(s) of this article can be found under https://doi.org/10.1002/adbi.201800002.

Prof. W. Jahnen-Dechent
Helmholtz-Institute for Biomedical Engineering
Biointerface Laboratory
Medical Faculty
RWTH Aachen University
52074 Aachen, Germany

Prof. T. Lammers
Department of Targeted Therapeutics
MIRA Institute for Biomedical Technology and Technical Medicine
University of Twente
7500 Enschede, The Netherlands

Prof. T. Lammers
Department of Pharmaceutics
Utrecht Institute for Pharmaceutical Sciences
Utrecht University
3584 Utrecht, The Netherlands

DOI: 10.1002/adbi.201800002

the cellular and molecular level, especially in the context of US-mediated burst or in conditions of inflammatory diseases. We have recently shown that PBCA-MB and their fragments primarily end up in tissue macrophages, especially in the liver, upon systemic administration in mice.[7] Liver macrophages (phagocytes) are critical components to ensure homeostasis of the body, and they integrate danger or other environmental signals by inflammatory (often termed "M1") or anti-inflammatory (often termed "M2") responses.[8] In this respect, liver macrophages are key regulators of systemic inflammation and hepatic diseases.[9]

In this study, we set out experiments to assess the functional effects of the hard-shell MB on monocytes/macrophages in general and liver macrophages in particular. We therefore investigated the impact of standard PBCA-MB, of PBCA-MB modified with streptavidin, and of PBCA-MB functionalized with the bioactive tripeptide arginylglycylaspartic acid (RGD) on human monocytes and macrophages in vitro. Moreover, as the liver is routinely exposed to US procedures, we assessed the potential toxicity of MB in combination with US-guided destruction. Furthermore, we investigated the effects of fluorescently labeled MB on hepatic immune cells in vivo upon intravenous administration in healthy mice as well as in mice subjected to liver injury.

2. Results and Discussion

2.1. MB Accumulate in the Liver and Are Cleared by Hepatic Monocytes and Macrophages

Gas-filled PBCA-MB were generated and fluorescently labeled (Figure S1A,B, Supporting Information) in order to trace the fate of MB within the body in mice. The micro-sized constructs were intravenously injected into mice, and whole-body scans based on combined microcomputed tomography/ fluorescence-mediated tomography (μCT/FMT) were performed.[10] The anatomical μCT data were used for an improved fluorescence reconstruction based on the accurate mouse shape and heterogeneous absorption and scattering maps (**Figure 1**A).[11] Organ segmentation was performed by delineating the organ boundaries in the μCT images (Figure 1B).[12] Fluorescence quantification revealed that the liver rapidly and predominantly harbored 40% of the injected dose of the MB shell constituents (Figure 1C). Half of the MB amount was still present in the liver after two hours. Most of the MB shell constituents were cleared from the body 24 h after injection.

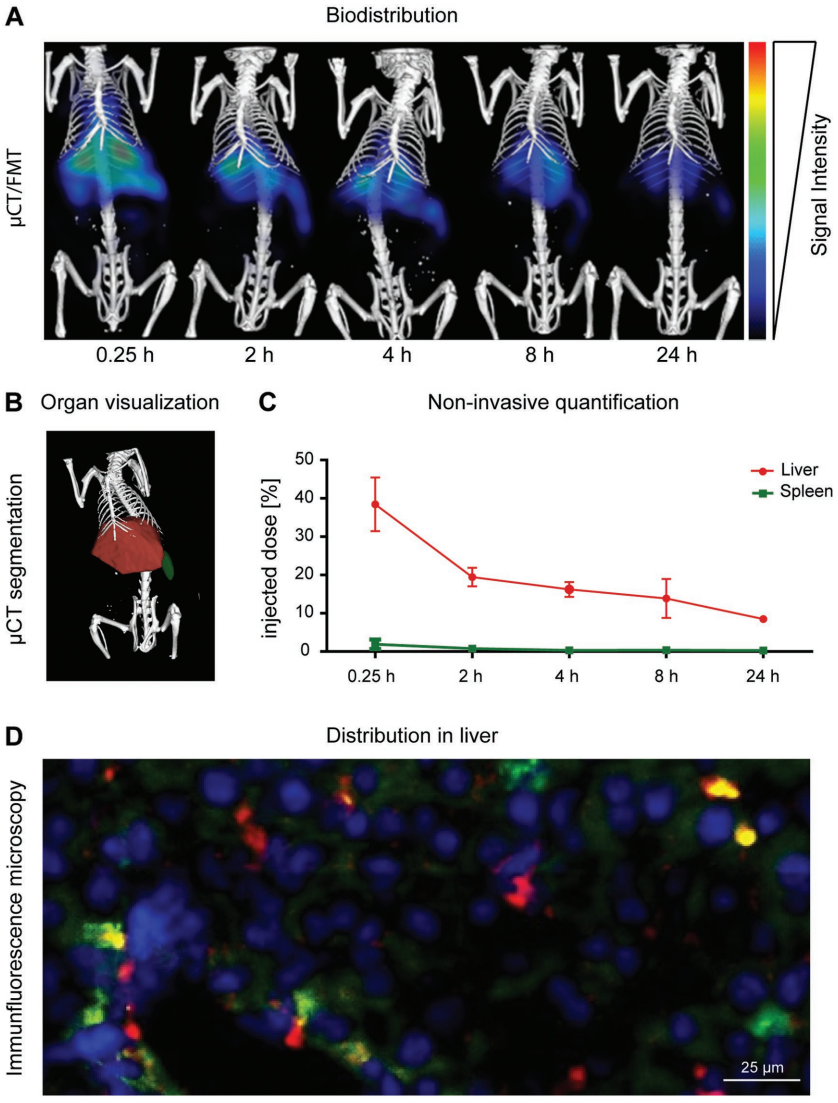

Figure 1. Microbubble (MB) distribution in vivo. 4×10^8 fluorescently labeled polymeric *n*-butyl cyanoacrylate (PBCA)-MB per kg body weight were injected intravenously into eight weeks old mice. A) Whole body scans generated using microcomputed tomography (μCT)/fluorescence-mediated tomography (FMT) imaging, representative images show uptake in liver and spleen. B) μCT images with organ segmentation showing liver (in red) and spleen (in green). C) Percentage of injected dose assessed by CT/FMT shown for liver and spleen. $n = 3$ mice. D) Immunfluorescence images of liver sections showing colocalization between MB (yellow) and Kupffer cells (F4/80, red) or monocyte-derived macrophages (CD11b, green). Cell nuclei were stained using 4′,6-diamidino-2-phenylindole (DAPI, blue).

Furthermore, we observed a delayed slight enrichment of MB shell constituents in spleen, but to a much lower extent than in liver (Figure 1C). Our data are well in accordance with a prior study using 2 μm hard-shell MB, although these MB showed a slightly higher accumulation in spleen.[7] Similarly, an independent study using gamma-counting demonstrated that the highest MB concentrations were observed in liver and lung, the latter being probably related to temporary retention in the pulmonary arterial system.[13] Furthermore, this work, based on radioactively labeled PBCA-MB of the same size and structure as in our current work, excluded that the fluorescent label accidentally detaches from the material. However, after two hours

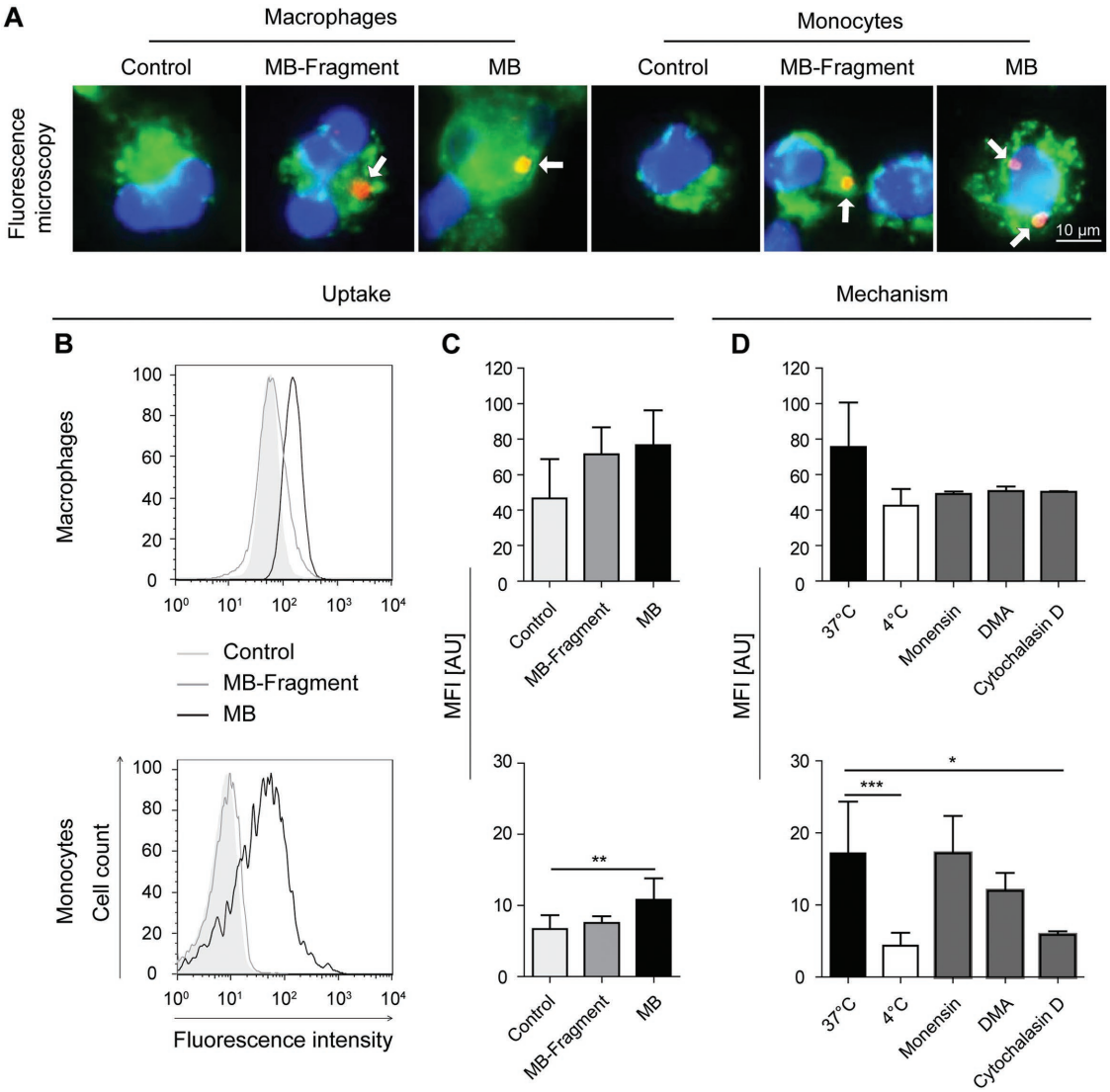

Figure 2. Uptake of fluorescent microbubbles (MB) by primary human myeloid immune cells. A) Representative images of cell type specific uptake of fluorescently labeled MB by human macrophages and monocytes. Cells were incubated for 60 min with MB (4×10^6 mL^{-1}, red, arrows), cell membranes were stained with wheat germ agglutinin (WGA-488, green) and nuclei using 4′,6-diamidino-2-phenylindole (DAPI, blue). Uptake of fluorescently labeled MB by human blood cells and macrophages studied after 60 min of incubation by flow cytometry based on B) quantification and C) mean fluorescence intensity (MFI). D) Investigation of the uptake mechanism by incubating immune cells with fluorescently labeled MB at 4 °C or by using inhibitors of endocytosis (Monensin), macropinocytosis (5-(*N*,*N*-dimethyl)amiloride hydrochloride (DMA), and phagocytosis (Cytochalasin D) 30 min prior to the incubation with fluorescently labeled MB at 37 °C. Data represent mean ± SD ($n = 6$ per condition); $*p < 0.05$, $**p < 0.01$, $***p < 0.001$ (two-tailed unpaired Student *t*-test).

MB concentration in the lung was strongly decreased leading to a reincrease in blood circulation.[13] To investigate which cells among the different cells in the liver take up the injected dose of MB, we performed immunohistochemistry analyses (Figure 1D). The MB are primarily found in Kupffer cells, the resident macrophages in the liver, characterized by high F4/80 expression, and to a lower extent in CD11b-expressing monocytes (or monocyte-derived macrophages), as shown by colocalization between MB and F4/80$^+$ or CD11b$^+$ cells (Figure 1D). In our study, low MB-related fluorescent signals were detected in other organs like spleen or lung, thus supporting that the MB are predominantly enriched in the liver and cleared by the hepatic myeloid cells (monocytes and macrophages).

2.2. Myeloid Cell-Specific Uptake Mechanisms of MB and Shell Fragments In Vitro

Due to the fact that MB primarily accumulated in the myeloid cells in the liver, we compared the cellular uptake efficiency of MB by human macrophages and monocytes in vitro using fluorescence microscopy and flow cytometric analysis. We studied the internalization of intact as well as fragmented MB by human primary macrophages and monocytes (**Figure 2**A–C; Figure S2A, Supporting Information) in comparison to human lymphocytes and granulocytes from peripheral blood (Figure S2B,C, Supporting Information). We used a concentration of intact and fragmented MB of 4×10^6 per mL that reflects an in

vivo concentration of 4×10^8 MB per kg body weight for the targeted drug delivery.[14] Fluorescence microscopic analysis indicated that the intact MB are rapidly fragmented either during or directly after internalization by human macrophages and monocytes, because the incubated MB or MB-fragments showed the same morphology after internalization (Figure 2A). While an increase in the mean fluorescence intensity (MFI) demonstrating efficient uptake was noted for MB and fragments in macrophages, a clear increase in MFI of human monocytes was only detectable after MB incubation but not for fragments (Figure 2B,C; Figure S2A, Supporting Information). Furthermore, very few lymphocytes and a minor fraction of primary granulocytes internalized MB and/or their fragments (Figure S2B,C, Supporting Information).

The incubation of primary human leukocytes with MB at 4 °C instead of 37 °C resulted in a suppression of MB internalization, indicating that the uptake is energy-dependent (Figure 2D).[15] To further investigate molecular mechanisms mediating the cell-specific uptake of MB, three important pathways for particle uptake,[16] namely receptor-mediated endocytosis, macropinocytosis or phagocytosis, were inhibited (Figure 2D). Monensin, a carboxylic ionophore that mediates proton movement across membranes, was used to block receptor-mediated endocytosis by entrapping receptor-ligand complexes.[17] Amiloride and its derivate 5-(*N*,*N*-dimethyl)amiloride hydrochloride (DMA) block macropinocytosis, because they function as selective inhibitors of the sodium-hydrogen exchange pump in the plasma membrane affecting the intracellular pH.[18] To block phagocytosis, we used Cytochalasin D, an agent known to block polymerization of actin.[19] Treatment with Cytochalasin D, but not with Monensin or DMA, led to a significant decrease in the uptake of MB by human monocytes (Figure 2D). Phagocytosis as the prime uptake mechanism was less clearly seen in the case of macrophages (although it has to be noted that these cells have a higher baseline MFI due to autofluorescence,[20] which may hamper the flow cytometry-based analysis). We excluded unspecific binding of complement proteins that might increase internalization efficiency of MB, by incubating cells in medium containing 5% human serum, instead of fetal calf serum (FCS), which is a source of complement protein (data not shown).

2.3. Transient Inhibition of Monocyte Migration by MB

We next tested consequences of MB internalization on the functional properties of the human monocytes and macrophages. Interestingly, we noted that the adherence of the human monocytes to cell culture plates was slightly reduced after internalization of MB, unlike if cells internalized 1 µm sized latex beads (Lx beads, **Figure 3**A,B). This prompted us to study the potential impact of MB on immune cell migration, a key feature for the monocyte recruitment to the inflammatory sites.[21] We determined the migration of the human monocytes in response to the functionalized MB in a transwell migration assay ("vertical cell migration"). Interestingly, spontaneous migration of monocytes was significantly inhibited by MB as well as by MB+RGD at 60 min after treatment (Figure 3C). At this time-point, only few macrophages had migrated (Figure S3A, Supporting Information). After 16 h, migration of the monocytes was increased compared to 1 h, but not substantially affected by MB (Figure 3C). We also tested horizontal migration of the human immune cells in vitro based on a scratch assay (performed on a confluent cell monolayer aiming to better mimic migration of the cells in vivo) (Figure 3D,E). The monocytes were incubated with MB using the conditions described before, and migration toward the cell-free gap was examined by analyzing images taken up to 24 h after scratch (Figure 3E). After 60 min scratching, twice as many monocytes migrated compared to the macrophages (Figure S3B, Supporting Information), illustrating their higher motility. Independent of the designated time-points, the treatment with regular or functionalized MB did not affect horizontal migration of the monocytes (Figure 3D). We observed that the internalization of MB affected the human monocytes by inhibiting their spontaneous migration, at least temporarily, without influencing viability. Next, we determined whether cytokine release as an additional functional property was altered after MB treatment. The macrophages were incubated with MB, soluble biotinylated RGD (2 nM mL^{-1}), MB functionalized with RGD or lipopolysaccharide (LPS, 1 µg mL^{-1}) for 24 h. Protein release of different pro- or anti-inflammatory cytokines remained unaffected by MB, whereas LPS that served as a positive control strongly induced inflammatory cytokines such as interleukin 1ß (IL-1ß) or tumor necrosis factor (Figure 3F). Furthermore, functionalization of MB did not change cell morphology (Figure S3C, Supporting Information) and did not alter surface expression level of antimyeloid related protein 8/14 (MRP8/14) and CD163, respectively,[22] as well as of MHC-II molecules (HLA-DR) (Figure S3D, Supporting Information). Although it was described before that the bioactive tripeptide RGD induced pronounced inflammatory conditions of human primary macrophages once coupled to a surface,[23] functionalization of MB by RGD did not induce inflammatory properties of the cells. In accordance with other studies, we used a relatively low concentration of soluble RGD, which had no activating effect on the human macrophages by itself.[24]

2.4. Cytotoxic Effects on Myeloid Cells during US-Provoked MB Disruption

We next analyzed the potential impact of MB uptake on the viability of human immune cell populations 24 h after MB incubation with two different concentrations (4×10^5 and 4×10^6 MB per mL). The viability of the human monocytes remained unaffected by MB; ethanol was used as a positive control for promoting cell death (**Figure 4**A,B). We next tested if the uptake of MB by human cells regularly results in MB fragmentation. We therefore exposed the human immune cells to US in vitro directly following MB uptake (Figure 4C). We hypothesized that those cells that have still incorporated intact MB should be susceptible to US-mediated MB burst and subsequent cell toxicity. Indeed, a part of MB remained intact after internalization by the monocytes, because US-guided destruction triggered cell death of monocytes (Figure 4D,E; Figure S4, Supporting Information). In contrast, the viability of mature human macrophages was not affected under identical experimental settings. To destroy hard-shell MB in this experimental setting, an US pulse with an acoustic pressure of mechanical index (MI)

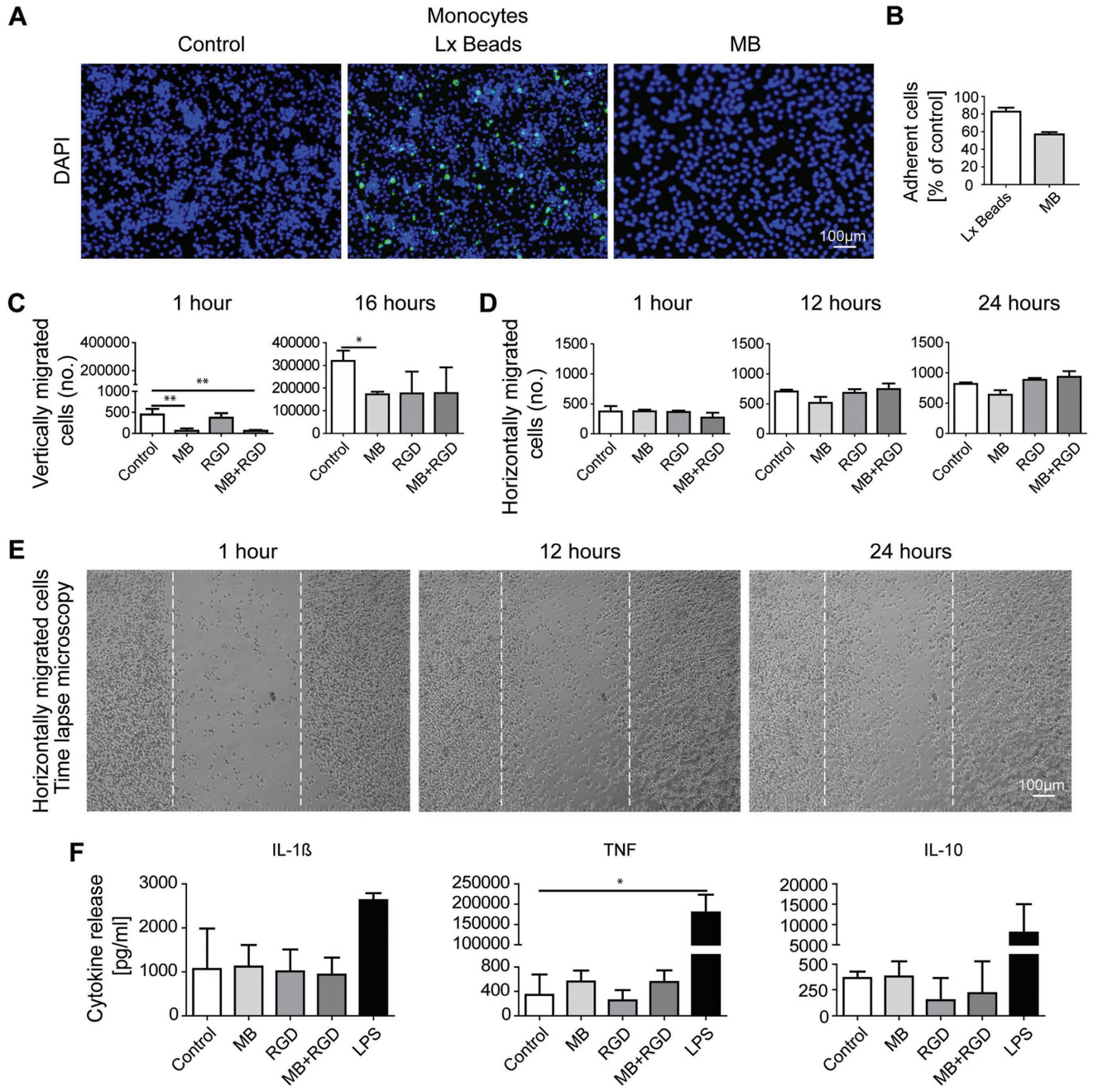

Figure 3. Influence of microbubbles (MB) on functional properties of monocytes. A) Human monocytes treated with MB (4×10^6 per mL), or latex (Lx) beads. Nuclei were stained using 4′,6-diamidino-2-phenylindole (DAPI, blue) and B) quantification of living adherent cells. C) Monocytes were incubated with MB, RGD (5 pmol) or a combination of MB functionalized with RGD for 60 min. Vertical migration of human monocytes for 60 min or 16 h. Statistical summary based on cell numbers by flow cytometry. D) Horizontal migration of human monocytes for 60 min, twelve hours, or 24 h. Flow cytometric analyses based on cell numbers and E) representative images using scratch assay analyses. F) Monocytes were incubated with MB, RGD, a combination of MB functionalized with RGD or lipopolysaccharides (LPS, 1 µg mL^{-1}) for 24 h. Cytokine release by human macrophages. Data represent mean ± SD ($n \geq 4$ per condition); $^*p < 0.05$, $^{**}p < 0.01$ (two-tailed unpaired Student *t*-test).

of 0.9 was applied resulting in an efficient destruction of the polymer-based MB (Figure 4C). It was reported earlier that the destruction of MB by high-intensity US can provoke cell-specific effects. For instance, in a prior study, the soft-shell MB remained intact after phagocytosis by neutrophils or monocytes and remained susceptible to US disruption, thereby affecting cell viability of neutrophils and monocytes.[25] In contrast, the macrophages in our study were not affected by US-guided MB burst, which could be related to cell-intrinsic features of macrophages, a more terminally differentiated cell compared to monocytes or neutrophils,[26] to the intracellular compartment in which MB are localized after phagocytosis or to the fact that MB are completely fragmented after internalization by human macrophages.

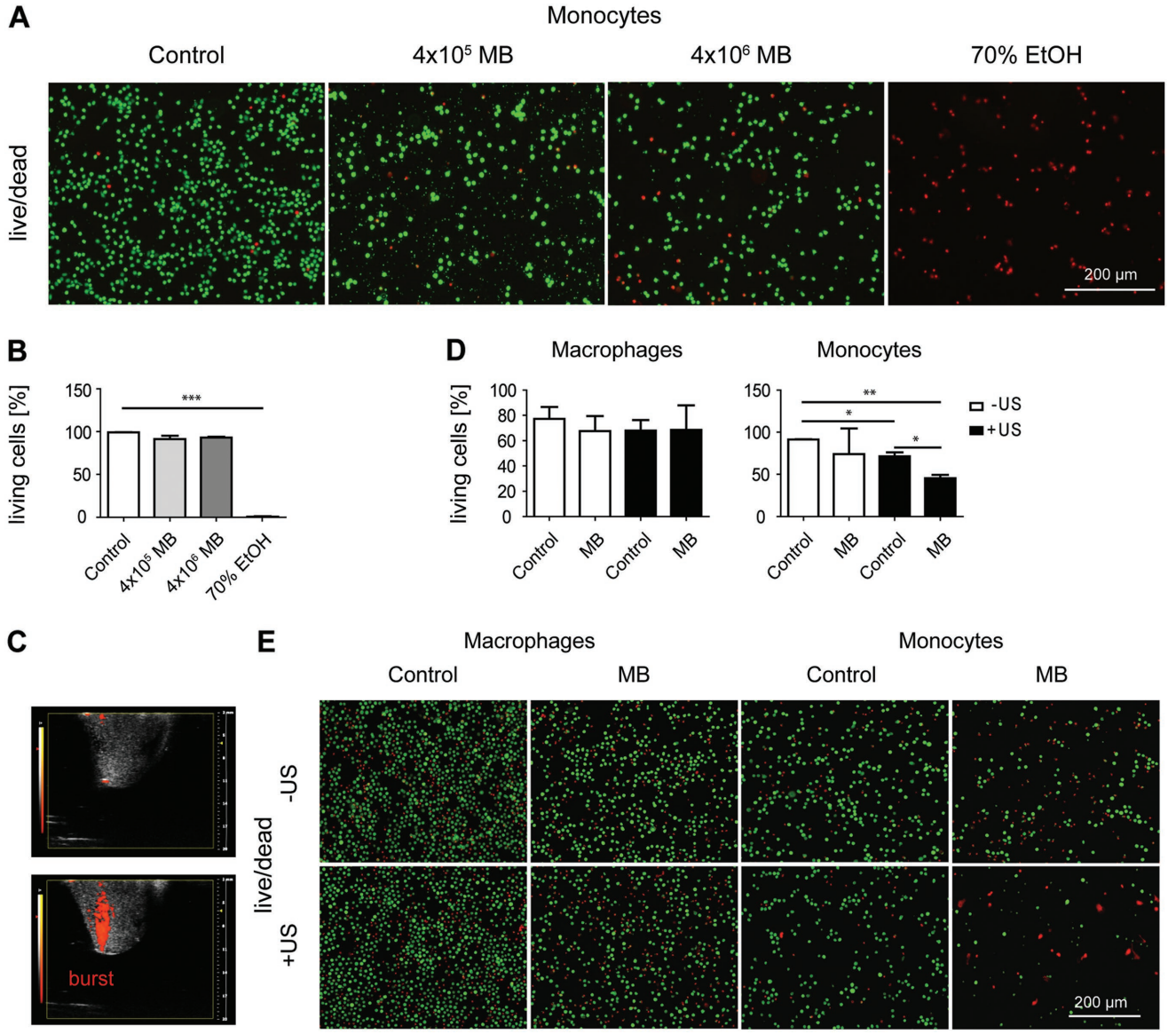

Figure 4. Cell type specific cytotoxic effects of microbubbles (MB) on human myeloid immune cells. A) Human monocytes incubated with different concentrations of MB for 24 h, untreated (control), or incubated for five minutes with 70% EtOH (positive control). The viable cells are stained with calcein-acetoxymethyl (green) and dead cells with propidium iodide (red). B) Statistical quantification of the live/dead staining using different concentrations of MB based on the percentage of untreated living cells. C) Macrophages and monocytes treated with MB (4×10^6 per mL) for 24 h and then embedded into 10% gelatin. Human cells with internalized MB (appear white) were exposed to an ultrasound (US)-guided burst of MB (red dots) for five minutes or remained untreated. D) Quantification of the live/dead staining after US-guided burst using percentage of living untreated cells. E) Live/dead staining of viable (green) or dead (red) cells after US-guided burst (+US) or without burst (–US). Data represent mean ± SD ($n = 6$ per condition); $^*p < 0.05$, $^{**}p < 0.01$, $^{***}p < 0.001$ (two-tailed unpaired Student *t*-test).

2.5. Evaluation of Hepatotoxic and Inflammatory Effects of MB In Vivo

The internalization of the micro-sized particles by human monocytes in vitro was accompanied by significantly increased cytotoxicity upon US treatment (Figure 4). To reveal whether these observations translate into US-mediated toxicity in vivo, we performed liver US of mice that had been injected with MB. As evidenced by US using brightness modulation (B mode) as well as contrast mode, MB and their fragments accumulated in the liver within minutes after injection (**Figure 5**A,B). We conducted a US-guided destructive pulse seven minutes after injection to destroy intact MB that had been attached to or internalized by hepatic phagocytes. The vast majority of MB were disrupted using a high-frequency destructive pulse illustrated by the mean intensity power (Figure 5C). After the first destructive pulse, no further accumulation of MB was observed, showing that most of the MB were rapidly and efficiently cleared from the circulation before the first destructive pulse. Importantly, neither MB nor MB+US treatment induced any type of overt liver damage, as analyzed by histology (Figure 5D) or the serum liver injury

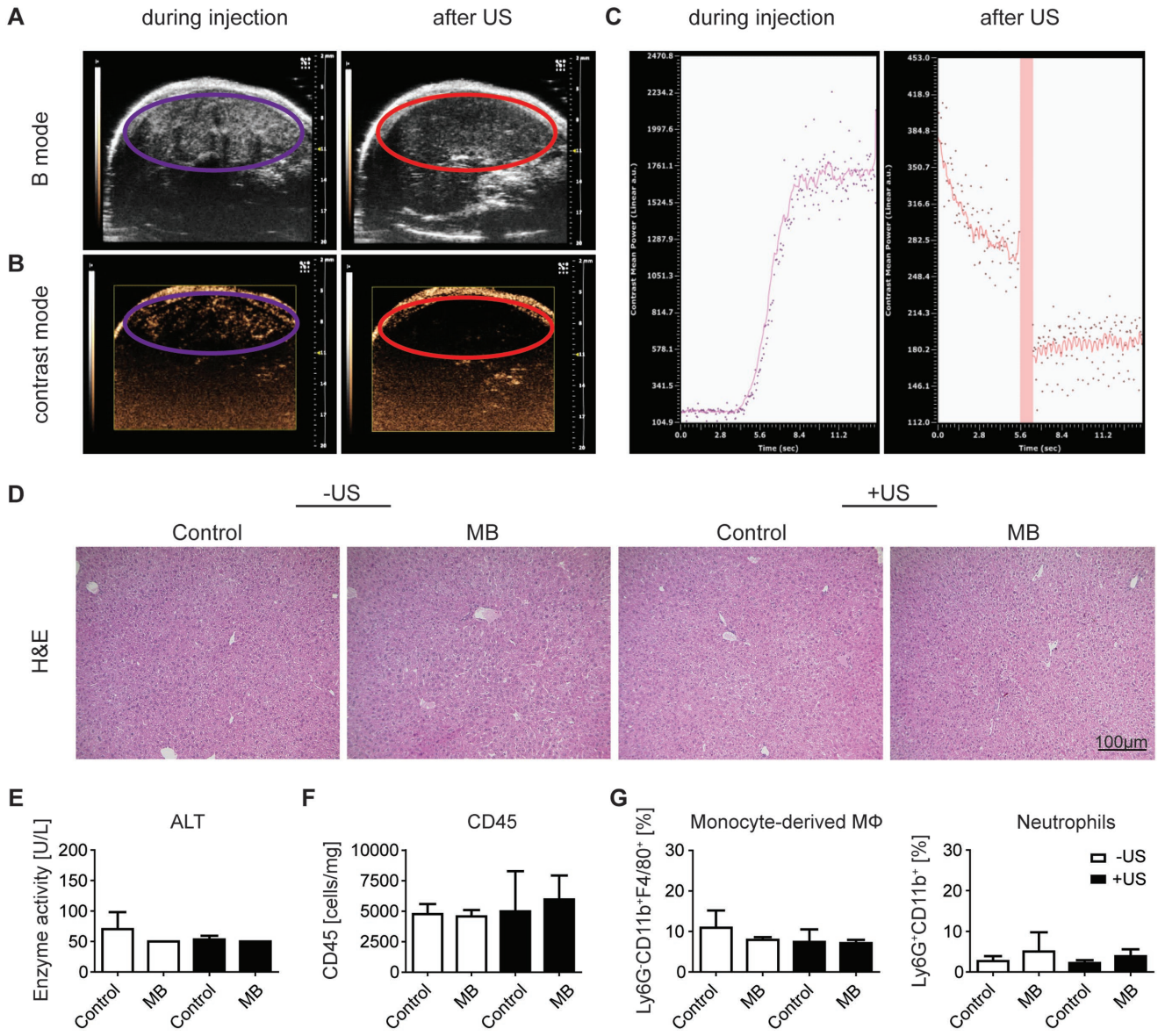

Figure 5. Effects of microbubble (MB) disruption on liver homeostasis in vivo. Eight weeks old C57BL/6 mice were injected intravenously with 4×10^8 fluorescently labeled MB per kg body weight or remained untreated. Mice were exposed to an ultrasound (US)-guided burst of MB (+US) or remained untreated (–US). After 24 h mice were sacrificed. A) US-based imaging of murine liver. 2D US image display using brightness modulation (B mode) and B) contrast mode during injection of MB (highlighted in purple circles) and after burst of MB (highlighted in red circles). C) Representative images of the mean contrast intensity (signal intensity) of MB during injection and after US-guided burst. D) Representative images of hematoxylin and eosin (H&E) staining of liver sections and E) serum levels of alanine aminotransferase (ALT) activity after exposition to a US-guided burst of MB (+US, black) or without (–US, white). F) Flow cytometric quantification of leukocyte cell number and G) flow cytometry-based quantification of inflammatory macrophages and neutrophils in the liver. Data represent mean ± SD ($n = 3$ per condition), two-tailed unpaired Student *t*-test.

indicator alanine aminotransferase (ALT, Figure 5E). These findings were further supported by the flow cytometric analysis of the hepatic leukocytes, which did not change upon treatment (Figure 5F). Interestingly, the monocyte-derived macrophages, which internalized MB and their fragments, as well as hepatic neutrophils (a sensitive indicator of liver injury), were unaffected upon MB treatment and in combination with US (Figure 5G). Similar results were obtained by the flow cytometric analysis for the blood cells (data not shown).

2.6. Analysis of Immunomodulatory Functions of MB and MB Burst during Liver Injury

These data demonstrated that MB or MB+US did not affect hepatic immune cells in homeostasis. However, we wanted to rule out that their functionality was altered in conditions of liver injury. Therefore, mice that had been exposed to MB with or without US treatment were challenged with an intraperitoneal (i.p.) injection of carbon tetrachloride (CCl_4), which induces a severe toxic liver damage, to examine

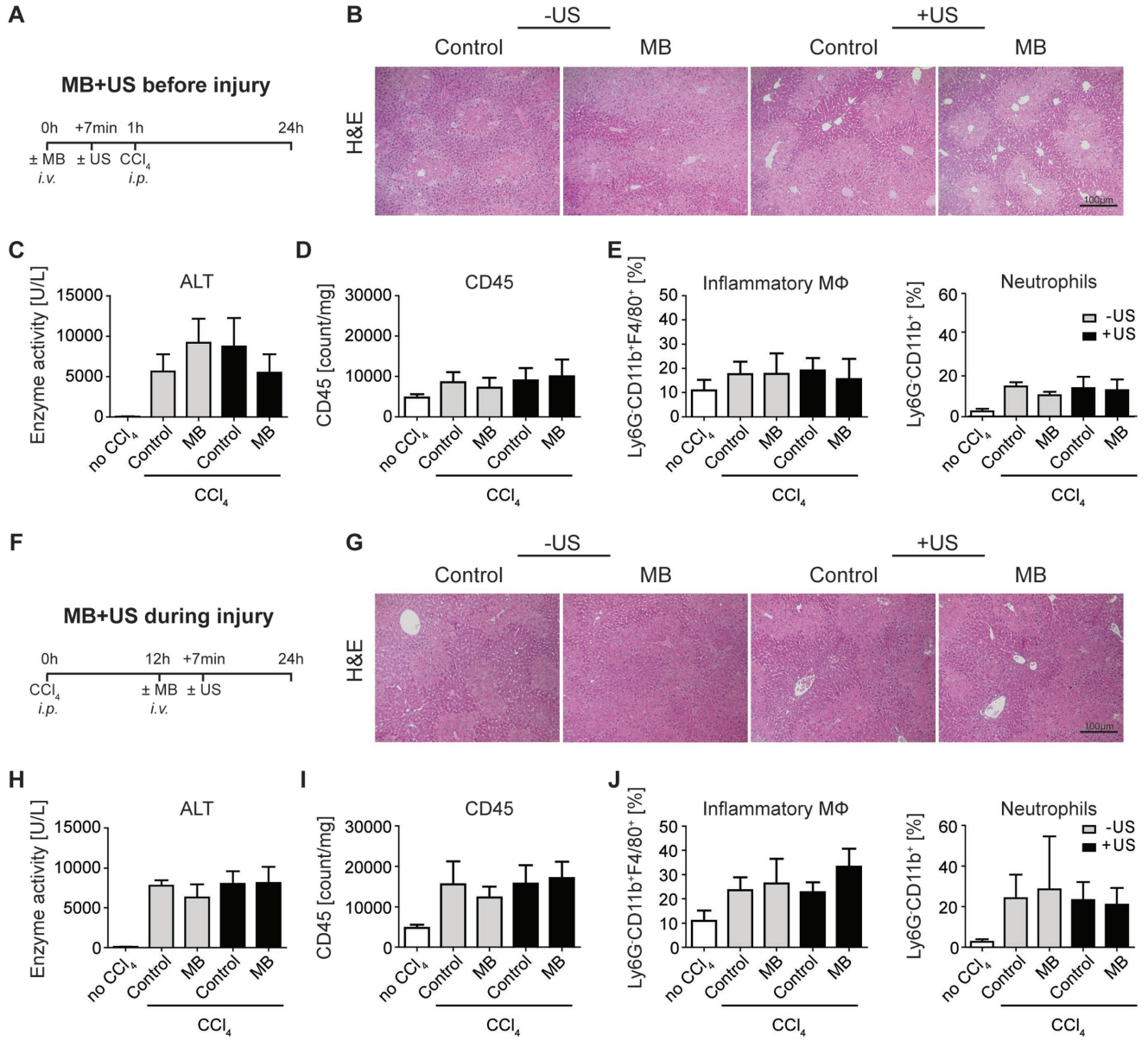

Figure 6. Effects of microbubbles (MB) on experimental liver injury in vivo. A) Eight weeks old C57BL/6 mice remained untreated or were injected intravenously (i.v.) with 4×10^8 fluorescently labeled MB per kg body weight followed by an ultrasound (US)-guided burst of MB after seven minutes. Mice were treated with the hepatotoxin CCl_4 intraperitoneally (i.p.) 60 min after MB injection and sacrificed after 24 h. B) Hematoxylin and eosin (H&E) staining of liver sections and C) alanine aminotransferase (ALT) activity reflecting liver injury after exposition to a US-guided burst of MB (+US, black) or without (–US, white). D) Flow cytometric quantifications of leukocytes, E) inflammatory macrophages, and neutrophils in the liver. F) Eight weeks old C57BL/6 mice were treated with the hepatotoxin CCl_4, followed twelve hours later by an (i.v.) injection of MB. Mice were exposed to a US-guided burst of MB after seven minutes and sacrificed after twelve h. G) H&E staining of liver sections and H) ALT activity measurements. I) Leukocyte cell numbers and J) inflammatory macrophages and neutrophils were analyzed by flow cytometry. Data represent mean ± SD ($n = 3$ per condition), two-tailed unpaired Student *t*-test.

whether MB impaired immune cells to react efficiently to liver injury (**Figure 6**A). This experiment revealed no overtly increased liver injury by histology (Figure 6B) or ALT levels (Figure 6C). Moreover, the hepatic leukocytes (Figure 6D) and inflammatory macrophages or neutrophils (Figure 6E) remained unaffected by prior MB and US treatment, suggesting that injury-mediated cell recruitment is not impaired by MB and shell constituents.

We next examined whether MB delivery and US burst during ongoing liver injury would affect liver damage or inflammation. Therefore, the mice were treated with CCl_4 to induce severe acute liver damage, followed by MB and US treatment at 12 h, when substantial injury is established (Figure 6F). MB treatment during progressive liver damage did not change overt liver injury as shown by histology (Figure 6G) and serum ALT (Figure 6H). Moreover, the recruitment of inflammatory cells

(Figure 6I), including macrophages and neutrophils (Figure 6J), to the liver remained unaffected.

We believe that our data have important implications for the future development of the hard-shell MB as drug carriers. Among many nano- and micro-sized carrier structures, there is the concern that either the material or the functionalization part might have additional, unwanted side effects on the immune system, especially in their prime target organ liver. This has been exemplarily demonstrated for gold nanorods, which affect the polarization of macrophages that internalize the rods,[27] or for selectin-mimicking polymers that affect the migration of macrophages.[28] The hard-shell MB offer the possibility for a targeting of phagocytes in solid organs,[7] and drug release from MB could even be tailored to distinct sites such as tumor tissue by US-guided disruption.[29] Although MB affect monocyte viability and migration in vitro, which had been previously demonstrated for the soft-shell MB as well,[30] they do not impair the viability or functionality of the hepatic myeloid cells in vivo, which represent their main cellular targets after systemic administration. Nonetheless, long(er) term and repetitive exposure need to be tested in future studies in order to confirm the favorable safety profile. Moreover, our study used primary human monocytes and macrophages in vitro side-by-side to extensive in vivo studies in healthy and diseased mice. While these data consistently support the immunological safety of the hard-shell MB, it cannot be excluded that murine and human immune cells, particularly in human liver, might show different responses. Thus, further in-depth analyses with human liver cells are warranted.

3. Conclusion

In this study, we comprehensively analyzed the immunological properties of MB, which were nonfunctionalized or surface-functionalized using Rhodamine-B, streptavidin, and RGD, on two different biological systems: murine hepatic immune cells and human primary leukocytes. Our data demonstrate that the MB exerted no activating effect on the human macrophages in vitro. Interestingly, the human myeloid cells showed different potential for uptake and migration of the hard-shell MB shell constituents. Monocytes internalized MB by phagocytosis, which transiently inhibited their migratory properties, and were modestly susceptible to the cytotoxic effects of MB during US-guided destruction. On the other hand, human macrophage viability and function remained unaffected after MB uptake. After i.v. injection in mice, MB preferentially accumulated in liver. Although MB were suitable to target immune cells in the liver, they did not cause overt hepatotoxicity, did not alter immune cell function and did not affect the inflammatory response to acute liver injury. Therefore, our data strongly support the further development of MB for multiple diagnostic, therapeutic, and theranostic applications, possibly also for the treatment of liver diseases or cancer. Combining MB that incorporate drugs and US-mediated MB disruption may provide options for targeted drug delivery without strong immunological bystander effects.

4. Experimental Section

Microbubble Preparation: The preparation of PBCA-MB by emulsion polymerization techniques was described before.[13] PBCA-MB were washed four times by flotation to remove unentrapped polymer. Fluorescently labeled MB were additionally prepared based on a one-step drug-loading procedure. Therefore, Rhodamine-B (AppliChem, Germany), which was dissolved in water, or 1,1,3,3,3,3-hexamethylindotricarbocyanine iodide (the higher wavelength (absorption max. 740 nm, emission max. 780 nm), which was required for the in vivo biodistribution studies, was added during the polymerization process. The MB were washed by flotation and their size and concentration were investigated by using a Multisizer 3 (Beckmann Coulter, Germany). The modified MB were prepared by coupling streptavidin (Merck, Germany) to the surface of a 10% hydrolysis of MB. Therefore, MB and fluorescently labeled MB were first treated with 0.1 N NaOH to introduce carboxyl groups and then 5×10^8 MB were dissolved in 10×10^{-3} M sodiumacetate (pH 4.5), incubated with 7.5 mg of 1-ethyl-3-(3-dimethylaminopropyl) carbodiimide (Merck, Germany) and 300 µg streptavidin for 60 min at room temperature and stirred overnight at 4 °C. To produce MB functionalized with streptavidin and RGD, 2 nM mL^{-1} of biotinylated RGD was added to MB coupled to streptavidin and incubated for five minutes until biotin and streptavidin built a strong complex. The MB were fragmented using an ultrasonic cleaner (UCS 200TH, VWR, USA) by sonicating 1 mL of the MB for 1 min at 60 W. The mean fragment size was 243 nm (compared to intact MB with a mean size of 1–3 µm). The concentration of the fragmented MB was $1.93 \times 10^{13} \pm 0.53 \times 10^{13}$ particles per mL.

Human Cells: Human primary blood leukocytes including granulocytes, lymphocytes, and monocytes were retrieved from healthy volunteers using dextran sedimentation. Peripheral blood mononuclear cells (PBMC) were isolated by Ficoll-based density gradient centrifugation as described before.[31] After centrifugation, PBMC were incubated at 37 °C for 30 min on bacterial grade Petri dishes at a density of 2.5 million cells per mL in cell culture medium (Roswell Park Memorial Institute medium, RPMI1640, PAA, Austria) with 1.5% heat-inactivated autologous serum, sterile-filtered using a 0.2 µm filter (Corning, USA) in a humidified incubator with 5% CO_2. Human monocytes become adherent, while lymphocytes remain in the supernatant. After removing the supernatant and washing with 37 °C RPMI1640, the monocytes were cultured for further seven days in RPMI1640 containing 5% autologous serum to obtain macrophages. Afterward, the adherent macrophages were put on ice for 20 min and then detached using a cell scraper (SPL, Korea). For the human in vitro experiments, 4×10^6 MB per mL medium were used that reflects an in vivo concentration of 4×10^8 MB per kg body weight based on the assumption that one mouse has a total body fluid volume of 2.5 mL. Informed signed consents were obtained from all healthy volunteers.

Mice: The C57BL/6J wild-type and hairless Balb/c nu/nu mice (used for µCT/FMT experiments) were housed in a specific pathogen-free environment. All experiments were done with male animals at the age of eight weeks that were carried out according to the guidelines of the federation of laboratory animal science associations (FELASA). For the in vivo studies, 4×10^8 MB per kg body weight were injected intravenously via the tail vein, based on earlier data on the targeted and triggered drug-delivery using polymer-based MB.[14] This dose equates to ≈80 µg PBCA (as assessed by weighing the dried mass after washing) per kg body weight (i.e., 2 µg PBCA per animal).

µCT/FMT Imaging: Balb/c nu/nu mice were injected intravenously with fluorescently labeled MB. A whole body-scan was performed using µCT scanning (Tomoscope Duo, CT Imaging Germany) followed by FMT imaging (FMT2500 LX, PerkinElmer, USA) as described earlier.[10] The total fluorescence intensity was evaluated by normalization to the total fluorescence intensity in the whole mouse 15 min after MB injection.

Staining of Liver Sections: Formalin-embedded liver sections were cut into 10 µm pieces, dried at room temperature for 2 h and washed trice with phosphate-buffered saline (PBS, PAA, Austria). Liver sections were stained with directly conjugated rat anti-mouse F4/80 and CD11b (both BD, Germany) in a moist chamber overnight. The samples were

washed three times for 5 min with PBS and mounted on cover slips using Vectashield mounting medium (Vector laboratories, USA). The fluorescently labeled MB (yellow), Kupffer cells (F4/80$^+$, red), monocyte-derived macrophages (CD11b$^+$, green) and cell nuclei (blue) were detected using an Axio Imager M2 (Zeiss, Germany).

Flow Cytometry: For human macrophages, cell surface markers were stained with directly conjugated mouse anti-human antibodies MRP8/14 (BMA biomedicals, Switzerland), anti-CD163 (R&D systems, USA), and anti-HLA-DR (BD, Germany). For mouse experiments, the hepatic leukocytes were isolated and stained for flow cytometry as described earlier.[27] Cell suspensions were filtered using a 100 µm mesh. To count cells, 2×10^4 counting beads (calibrate beads, BD, Germany) were added to all samples. The flow cytometric data are given as MFI. Human blood cell populations are represented in absolute numbers or as percentages of leukocytes. Murine cell populations are shown in absolute numbers calculated from organ weight or as percentages of leukocytes. Using this methodology for calculation, a healthy mouse liver (≈2 g) contains ≈1.25 million Kupffer cells.

Uptake Studies and Microscopy: Human monocytes (two million cells per mL) and macrophages (one million cells per mL) were incubated for 60 min with fluorescently labeled MB (4×10^6 per mL) in RPMI1640 and 5% FCS (PAA, Austria) at 37 °C or 4 °C under continuous shaking conditions (500 rpm) in 1.5 mL tubes on a Thermomixer comfort (Eppendorf, Germany). For studies of the uptake mechanism, the cells were incubated with the inhibitors Monensin (100 µg mL^{-1}), DMA (50×10^{-6} M), or Cytochalasin D (40×10^{-6} M, all from Merck, Germany) for 30 min prior to uptake analysis. The cells were washed with PBS and counted using a FACS Canto II (BD, Germany). Data were analyzed using FlowJo (TreeStar, USA). For plasma membrane and nuclear staining, human monocytes and macrophages were first subjected to an uptake study with fluorescently labeled MB. They were put on glass slides coated with poly-L-lysine (Merck, Germany). Adherent cells were treated with a mix of 5 µg mL^{-1} wheat germ agglutinin Alexa Fluor-488 conjugate (invitrogen, UK) and 100 ng mL^{-1} 4′,6-diamidino-2-phenylindole (invitrogen, UK) for 30 min. They were washed three times with Hank's balanced salt solution (PAA, Austria) and mounted on cover slips using Vectashield mounting medium (Vector laboratories, USA). The fluorescently labeled MB (red channel) and labeled cells (green and blue channel) were detected using an Axio Imager M2 (Zeiss, Germany).

Migration Studies and Time Lapse Microscopy: Human macrophages and monocytes were incubated with MB to allow MB uptake. Afterward, two million monocytes or one million macrophages were resolved in 200 µL RPMI1640 with 1% FCS and added on top of a transwell insert (Millipore, USA) that was inserted on a 24-well plate (Greiner, Austria) containing 800 µL of RPMI1640 and 1% FCS at the bottom. Cells migration was studied after 60 min or 16 h after incubation at 37 °C. Cells that migrated to the bottom of the 24-well plate were counted by flow cytometry. To analyze horizontal cell migration behavior into a defined area, an experiment similar to a "scratch" assay was performed using silicone inserts for self-insertion (ibidi, Germany). To this end, human monocytes and macrophages were treated with functionalized MB for 24 h, washed with PBS, and resolved in 1 mL RPMI1640 with 1.5% autologous serum on 24-well plates containing the culture inserts. Once the cells became adherent, the inserts were removed resulting in a cell layer with a 500 µm cell-free gap. Using an Axio Observer Z1 equipped with an Axio Cam MR and an XLmulti S1 DARK LS incubator (Zeiss, Germany), images of migrating cells were taken at the designated time-points. The data were processed with the ZEN pro.2012 software (Zeiss, Germany). Video sequence analysis was performed using Imaris (version 7.7.2, Switzerland) and ilastik software (version 1.1.2, Germany).

Cytokine Release: The release of different cytokines by human macrophages into the cell culture medium was quantified using a bead-based multiplex assay (ThermoFisher, USA). All results are based on the comparison to the untreated control. 1 µg per mL LPS (Merck, Germany) served as a control.

In Vitro Ultrasound and Cell Viability Assessment: Human monocytes and macrophages were incubated with MB in RPMI1640 and 5% FCS for 60 min and transferred to a solidified matrix of 10% gelatin including 1 mL inlets to insert the medium containing cells. The solidified gelatin is required to ensure an optimal transmission during US treatment. US imaging was performed using a preclinical US device (Vevo 2100, VisualSonics, Canada) with an MS250 transducer (VisualSonics, Canada). MB were destroyed by applying destructive US at a frequency of 16 MHz with an MI of 0.9 (corresponding to 100% power). Afterward, cells were taken out of the inlets, washed with PBS, and transferred to 24-well plates. Live/dead staining including calcein-acetoxymethyl for staining of viable cells and propidium-iodide for labeling dead cells was done according to the instructions of the manufacturer (Life Technologies, USA). Data processing was performed using ilastik software (version 1.1.2, Germany).

Liver Injury Model: 4×10^8 MB per kg body weight were injected intravenously at a volume of 125 µL in eight weeks old c57BL/6 mice. Acute liver injury was induced by intraperitoneal injection of 0.6 mL per kg CCl_4 (Merck, Germany) 24 h before euthanizing mice.

In Vivo Ultrasound: The mice were anesthetized using isoflurane and the hair were removed at the abdomen before performing US imaging using the Vevo2100 system with the MS250 transducer. The liver was focused in B mode- US imaging and 10^7 MB were injected intravenously that directly enriched in the liver. A first destructive pulse at a frequency of 18 MHz with an MI of 0.7 (corresponding to 100% power) was induced after seven minutes to destroy MB in the liver, resulting in a decreased signal of contrast mean power. This was followed by a continuous imaging with an MI of 0.03 (corresponding to 4% power) for five minutes and a second destructive pulse at 100% power to ensure that all MB were destroyed in the liver during the first destructive pulse.

Statistical Analysis: The data presented as mean ± SD, $n \geq 3$. All outliers were included in the analyses. p-values are calculated using two-tailed unpaired Student *t*-test. Significance was defined as $^*p < 0.05$, $^{**}p < 0.01$, $^{***}p < 0.001$. Statistical analysis was carried out using GraphPad prism 5.

Supporting Information

Supporting Information is available from the Wiley Online Library or from the author.

Acknowledgements

This study was funded by the German Research Foundation (Ta434/3-1, Ta434/5-1, SFB/TRR57 P09 to F.T.), by the START program of the Medical Faculty of the RWTH Aachen University (to M.B.), by the Wilhelm Sander Foundation (to M.B.) and by ERCStG-309495 (to T.L.). The authors gratefully acknowledge Dr. S. Fokong for assistance with microbubble preparation and characterization, Dr. J. Ehling and A. Rix for excellent guidance during ultrasound treatment.

Conflict of Interest

F.K. is consultant of Bracco, shares IP on fluorescent PBCA-MB with FUJIFILM VisualSonics and is co-owner and advisor on the invivoContrast GmbH. The other authors disclose no conflict of interest.

Keywords

cell migration, inflammation, liver, macrophages, microbubbles, ultrasound

Received: January 4, 2018
Revised: February 27, 2018
Published online: April 16, 2018

[1] A. L. Klibanov, J. A. Hossack, *Invest Radiol.* **2015**, *50*, 657.
[2] M. Claudon, C. F. Dietrich, B. I. Choi, D. O. Cosgrove, M. Kudo, C. P. Nolsoe, F. Piscaglia, S. R. Wilson, R. G. Barr, M. C. Chammas, N. G. Chaubal, M. H. Chen, D. A. Clevert, J. M. Correas, H. Ding, F. Forsberg, J. B. Fowlkes, R. N. Gibson, B. B. Goldberg, N. Lassau, E. L. Leen, R. F. Mattrey, F. Moriyasu, L. Solbiati, H. P. Weskott, H. X. Xu, *Ultrasound Med Biol.* **2013**, *39*, 187.
[3] P. Koczera, L. Appold, Y. Shi, M. Liu, A. Dasgupta, V. Pathak, T. Ojha, S. Fokong, Z. Wu, M. van Zandvoort, O. Iranzo, A. J. C. Kuehne, A. Pich, F. Kiessling, T. Lammers, *J. Controlled Release* **2017**, *259*, 128.
[4] BR55 in Prostate Cancer: An Exploratory Clinical Trial, https://clinicaltrials.gov/ct2/show/NCT01253213 (accessed: Sept 2017).
[5] N. T. Blum, A. Yildirim, R. Chattaraj, A. P. Goodwin, *Theranostics* **2017**, *7*, 694.
[6] A. Rix, S. Fokong, S. Heringer, R. Pjontek, L. Kabelitz, B. Theek, M. A. Brockmann, M. Wiesmann, F. Kiessling, *Invest. Radiol.* **2016**, *51*, 767.
[7] C. Ergen, F. Heymann, W. Al Rawashdeh, F. Gremse, M. Bartneck, U. Panzer, R. Pola, M. Pechar, G. Storm, N. Mohr, M. Barz, R. Zentel, F. Kiessling, C. Trautwein, T. Lammers, F. Tacke, *Biomaterials* **2017**, *114*, 106.
[8] A. M. Mowat, C. L. Scott, C. C. Bain, *Nat. Med.* **2017**, *23*, 1258.
[9] O. Krenkel, F. Tacke, *Nat. Rev. Immunol.* **2017**, *17*, 306.
[10] F. Gremse, D. Doleschel, S. Zafarnia, A. Babler, W. Jahnen-Dechent, T. Lammers, W. Lederle, F. Kiessling, *J. Visualized Exp.* **2015**, e52770.
[11] F. Gremse, B. Theek, S. Kunjachan, W. Lederle, A. Pardo, S. Barth, T. Lammers, U. Naumann, F. Kiessling, *Theranostics* **2014**, *4*, 960.
[12] F. Gremse, M. Stark, J. Ehling, J. R. Menzel, T. Lammers, F. Kiessling, *Theranostics* **2016**, *6*, 328.
[13] M. Palmowski, B. Morgenstern, P. Hauff, M. Reinhardt, J. Huppert, M. Maurer, E. C. Woenne, S. Doerk, G. Ladewig, J. W. Jenne, S. Delorme, L. Grenacher, P. Hallscheidt, G. W. Kauffmann, W. Semmler, F. Kiessling, *Invest. Radiol.* **2008**, *43*, 162.
[14] S. Fokong, B. Theek, Z. Wu, P. Koczera, L. Appold, S. Jorge, U. Resch-Genger, M. van Zandvoort, G. Storm, F. Kiessling, T. Lammers, *J. Controlled Release* **2012**, *163*, 75.
[15] M. Bartneck, H. A. Keul, S. Singh, K. Czaja, J. Bornemann, M. Bockstaller, M. Moeller, G. Zwadlo-Klarwasser, J. Groll, *ACS Nano* **2010**, *4*, 3073.
[16] M. A. Dobrovolskaia, S. E. McNeil, *Nat. Nanotechnol.* **2007**, *2*, 469.
[17] T. Wileman, R. L. Boshans, P. Schlesinger, P. Stahl, *Biochem. J.* **1984**, *220*, 665.
[18] K. J. Sandgren, J. Wilkinson, M. Miranda-Saksena, G. M. McInerney, K. Byth-Wilson, P. J. Robinson, A. L. Cunningham, *PLoS Pathog.* **2010**, *6*, e1000866.
[19] S. D. Conner, S. L. Schmid, *Nature* **2003**, *422*, 37.
[20] M. Bartneck, K. M. Scheyda, K. T. Warzecha, L. Y. Rizzo, K. Hittatiya, T. Luedde, G. Storm, C. Trautwein, T. Lammers, F. Tacke, *Biomaterials* **2015**, *37*, 367.
[21] F. Heymann, F. Tacke, *Nat. Rev. Gastroenterol. Hepatol.* **2016**, *13*, 88.
[22] A. Gratchev, J. Kzhyshkowska, J. Utikal, S. Goerdt, *Scand. J. Immunol.* **2005**, *61*, 10.
[23] M. Bartneck, C. Skazik, N. E. Paul, J. Salber, D. Klee, G. Zwadlo-Klarwasser, *Macromol. Biosci.* **2014**, *14*, 411.
[24] C. Moon, J. R. Han, H. J. Park, J. S. Hah, J. L. Kang, *Respir. Res.* **2009**, *10*, 18.
[25] J. R. Lindner, P. A. Dayton, M. P. Coggins, K. Ley, J. Song, K. Ferrara, S. Kaul, *Circulation* **2000**, *102*, 531.
[26] C. Varol, A. Mildner, S. Jung, *Annu. Rev. Immunol.* **2015**, *33*, 643.
[27] M. Bartneck, T. Ritz, H. A. Keul, M. Wambach, J. Bornemann, U. Gbureck, J. Ehling, T. Lammers, F. Heymann, N. Gassler, T. Ludde, C. Trautwein, J. Groll, F. Tacke, *ACS Nano* **2012**, *6*, 8767.
[28] K. E. Moog, M. Barz, M. Bartneck, F. Beceren-Braun, N. Mohr, Z. Wu, L. Braun, J. Dernedde, E. A. Liehn, F. Tacke, T. Lammers, H. Kunz, R. Zentel, *Angew. Chem., Int. Ed. Engl.* **2017**, *56*, 1416.
[29] S. Eggen, S. M. Fagerland, Y. Morch, R. Hansen, K. Sovik, S. Berg, H. Furu, A. D. Bohn, M. B. Lilledahl, A. Angelsen, B. Angelsen, C. de Lange Davies, *J. Controlled Release* **2014**, *187*, 39.
[30] B. A. Kaufmann, J. M. Sanders, C. Davis, A. Xie, P. Aldred, I. J. Sarembock, J. R. Lindner, *Circulation* **2007**, *116*, 276.
[31] M. Bartneck, F. M. Peters, K. T. Warzecha, M. Bienert, L. van Bloois, C. Trautwein, T. Lammers, F. Tacke, *Nanomedicine* **2014**, *10*, 1209.